Available online at www.sciencedirect.com
SCIENCE DIRECT
ELSEVIER
Ocean Engineering 32 (2005) 961–985
OCEAN ENGINEERING
www.elsevier.com/locate/oceaneng

Extended energy-balance-equation wave model for multidirectional random wave transformation

Hajime Mase[a,*], Kazuya Oki[b], Terry S. Hedges[c], Hua Jun Li[d]

[a] *Disaster Prevention Research Institute, Kyoto University, Gokasho, Uji, Kyoto 611-0011, Japan*
[b] *Department of Urban and Environmental Engineering, Kyoto University, Yoshida-Honmachi, Kyoto 606-8501, Japan*
[c] *Department of Civil Engineering, University of Liverpool, Brownlow Street, Liverpool L69 3GQ, UK*
[d] *College of Engineering, Ocean University of China, 23 Hongkong East Road, Qingdao 266071, China*

Received 9 June 2004; accepted 13 October 2004
Available online 20 December 2004

Abstract

This study extends an energy-balance-equation wave model (a phase-averaging wave model) for multidirectional random wave transformations to account for wave shoaling, refraction, diffraction, reflection and breaking. Quadratic upstream interpolation for convective kinematics is used in the discretization to reduce numerical diffusion.

Predictions using the present wave model are compared with Sommerfeld's solutions for wave transformation through a gap between breakwaters, experimental observations for wave transformation due to a circular shoal, and field measurements for waves behind a breakwater. The results of these comparisons show fairly good agreement.

Keywords: Wave transformation model; Multidirectional random waves; Energy balance equation; Wave model; QUICK

1. Introduction

In the design of shore protection, it is necessary to estimate the nearshore wave conditions. Sea waves propagate from offshore to the beach and change their heights, lengths and directions according to the particular bathymetry and the presence of currents

* Corresponding author. Tel.: +81 774 38 4146; fax: +81 774 38 4321.
E-mail address: mase@kaigan.dpri.kyoto-u.ac.jp (H. Mase).

0029-8018/$ - see front matter
doi:10.1016/j.oceaneng.2004.10.015

and structures. Shoaling, refraction, diffraction, reflection and wave breaking may all occur. Since sea waves are random, accurate prediction of their transformation by these combined processes is difficult.

There are various theories and transformation models for nearshore waves. Each of the theories and models has certain advantages and limitations with respect to its applicability. Their appropriateness will depend on the relative importance of the various physical processes and the detail required at the target coastal site.

Mase and Kitano (2000) summarized the various random wave transformation models. Among them, the Boussinesq family falls within the refined time domain class of models. They give detailed information on wave profiles, wave set-up, averaged wave-induced currents and so on, by solving the continuity equations of mass and momentum (Peregrine, 1967; Madsen et al., 1991, 1997a,b; Nwogu, 1993; Wei et al., 1995; Gobbi and Kirby, 1999). Boussinesq wave models are currently confined to applications involving relatively small sea areas due to computation time and memory requirements. However, this restriction may ease with the further development of computers.

Wave prediction models based on the energy balance equation or wave action equation fall within the frequency domain class of models. They are suitable for applications involving large sea areas. The calculated quantities are the spectral energy densities or wave actions, which are phase averaged quantities slowly varying over several wavelengths. The wave forecasting and hindcasting models of WAM (WAMDI group, 1988) and SWAN (Booij et al., 1996) are based on the non-stationary phase averaging equation with source terms. Originally, phase averaging wave models did not account for wave diffraction. Recently, however, attempts have been made to introduce wave diffraction effects. The method adopted by Resio (1988) was to smooth the energy density, $S(f,\theta)$, at a point of (i,j), as $S^{ij}(f_n,\theta_k)=\sum_{p=-2}^{p=+2}\sum_{q=-1}^{q=+1}\varepsilon_{pq}S^{i(j+p)}(f_n,\theta_{k+q})$ where ε_{pq} are weight coefficients. Booij et al. (1997), Rivero et al. (1997) and Holthuijsen et al. (2003) introduced the diffraction effect into the characteristic velocities through the wave number containing the second derivative of wave amplitude with respect to the spatial coordinates. Mase (2001) directly introduced a diffraction term, formulated from a parabolic approximation wave equation, into the energy balance equation. The resulting formulation is easy to solve and the numerical scheme is very stable. In the model proposed by Mase (2001), the energy densities are smoothed at places where they are concentrated. Although the smoothing of energy densities is similar to the treatment by Resio (1988), the arbitrariness is removed from the coefficient ε_{pq}, the number of components p and q, and the location of the smoothing to be done. In the model employing the revised characteristic velocities, a smoothing technique for spectral density instead of wave amplitude is needed for numerical stability.

The first order upwind difference scheme employed by Mase (2001) is numerically stable due to numerical diffusion. The numerical diffusion term represented by the second derivative is similar to the wave diffraction term. Nevertheless, in order to suppress numerical diffusion separately from the effect of wave diffraction, quadratic upstream interpolation for convective kinematics (QUICK), proposed by Leonard (1979), is employed in the present wave model using an *Ex*tended *E*nergy-*B*alance-*E*quation with a *D*iffraction term, referred to here as the ExEBED wave model.

First, the effect of high-order differentiation is checked against the first-order solution for a simple case of wave transformation. Secondly, the prediction using the ExEBED wave model is compared with the Sommerfeld theory for the case of wave transformation through a gap between breakwaters in order to determine a suitable coefficient for the diffraction term, and the computed spatial wave height distributions given by the ExEBED model are shown together with Sommerfeld's solutions. Thirdly, the predictions provided by the ExEBED model are compared with the experimental results for wave transformation due to a circular shoal and with the observed wave heights behind a breakwater at a field site.

2. Wave model based on an energy-balance-equation with diffraction term (the EBED wave model)

For steady-state conditions, the energy balance equation with an energy dissipation term is written as

$$\frac{\partial(v_x S)}{\partial x} + \frac{\partial(v_y S)}{\partial y} + \frac{\partial(v_\theta S)}{\partial \theta} = -\varepsilon_b S \tag{1}$$

where $S = S(f, \theta)$ is the directional wave spectral density, (x,y) are the horizontal coordinates, θ is the wave direction measured counterclockwise from the x-axis, ε_b is the coefficient of energy dissipation, and the characteristic velocities,(v_x, v_y, v_θ), are defined as follows

$$(v_x, v_y, v_\theta) = \left\{ C_g \cos\theta,\ C_g \sin\theta,\ \frac{C_g}{C}\left(\sin\theta \frac{\partial C}{\partial x} - \cos\theta \frac{\partial C}{\partial y}\right) \right\} \tag{2}$$

where C is the wave celerity and C_g is the group velocity.

A basic form of parabolic wave equation including a dissipation term may be written as follows

$$2\mathrm{i}kCC_g A_x + \mathrm{i}(kCC_g)_x A + (CC_g A_y)_y = -\mathrm{i}kC\varepsilon_b A \tag{3}$$

where k is the wave number and A is the complex amplitude (see, for example, Radder, 1979; Kirby and Dalrymple, 1986). By multiplying Eq. (3) by A^* (the conjugate of A) and adding the conjugate of Eq. (3) multiplied by A, the resulting equation yields:

$$(C_g|A|^2)_x - \frac{\mathrm{i}}{2\omega}\{(CC_g|A|_y^2)_y - 2CC_g A_y A_y^*\} = \varepsilon_b |A|^2 \tag{4}$$

Satisfying the real and imaginary parts of Eq. (4) yields Eqs. (5) and (6):

$$(C_g|A|^2)_x = -\varepsilon_b|A|^2 \tag{5}$$

$$(CC_g|A|_y^2)_y - 2CC_g A_y A_y^* = 0 \tag{6}$$

Since the wave energy $E \propto |A|^2$, Eq. (5) denotes conservation of wave energy. Although it is impossible to rewrite $A_y A_y^*$ in Eq. (6) in terms of wave energy, it can be approximated by $E_{yy}/4$. Thus:

$$(C_g E)_x = -\varepsilon_b E \tag{7}$$

$$(CC_g E_y)_y - CC_g E_{yy}/2 \cong 0 \tag{8}$$

Having compared Eq. (7) with Eq. (1) and replaced wave energy E by spectral density S, Mase (2001) proposed a modified energy balance equation with a wave diffraction term as follows

$$\frac{\partial(v_x S)}{\partial x} + \frac{\partial(v_y S)}{\partial y} + \frac{\partial(v_\theta S)}{\partial \theta} = \frac{\kappa}{2\omega}\left\{(CC_g \cos^2\theta S_y)_y - \frac{1}{2}CC_g \cos^2\theta S_{yy}\right\} - \varepsilon_b S \tag{9}$$

in which the nearly zero term

$$(CC_g \cos^2\theta S_y)_y - \frac{1}{2}CC_g \cos^2\theta S_{yy} \cong 0 \tag{10}$$

has been added to the energy balance equation. Coefficient κ is a free parameter to be optimized in order to change the degree of diffraction. In the previous study of Mase (2001), $\kappa = 2.5$ was adopted. The method of adding terms which become identically zero at some condition is similar to the methods employed by Madsen et al. (1991) and Kaihatu and Kirby (1998) to improve the properties of the Boussinesq equations.

3. Discretization of the wave equation

Fig. 1 shows the grid system used in the discretization. The first term on the left-hand-side of Eq. (9) is discretized as follows:

$$\frac{\partial(v_{x_n} S)}{\partial x} = (S_n^{ijk} v_{x_n}^{(i+1)jk} - S_n^{(i-1)jk} v_{x_n}^{ijk})/\delta x \tag{11}$$

where i and j denote the grid positions in x and y, respectively, n is the frequency number and k is the wave direction number.

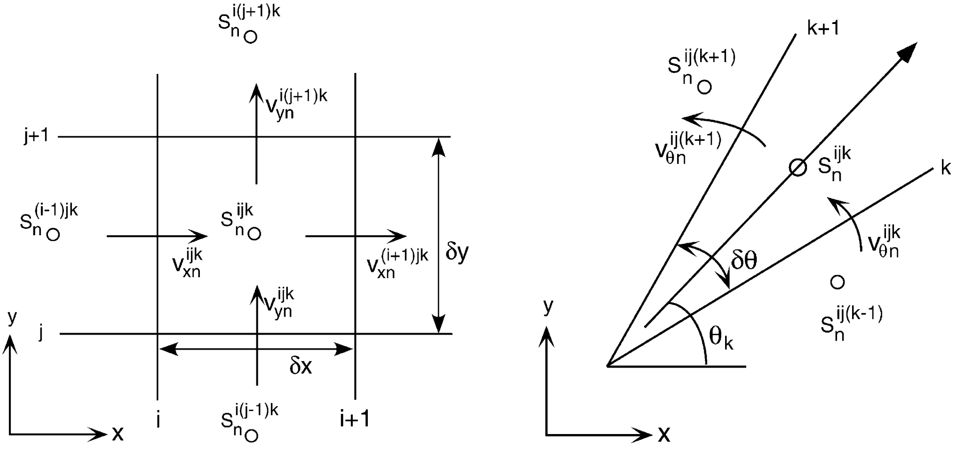

Fig. 1. Grid system.

The second term is discretized using the QUICK scheme (Leonard, 1979):

$$
\begin{aligned}
\frac{\partial(v_{y_n}S)}{\partial y} = \frac{1}{16\delta y}\{ & v_{y_n}^{i(j+1)k}(-S_n^{i(j+2)k} + 9S_n^{i(j+1)k} + 9S_n^{ijk} - S_n^{i(j-1)k}) \\
& - v_{y_n}^{ijk}(-S_n^{i(j+1)k} + 9S_n^{ijk} + 9S_n^{i(j-1)k} - S_n^{i(j-2)k})\} \\
& + \frac{\beta}{16\delta y}\{|v_{y_n}^{i(j+1)k}|(S_n^{i(j+2)k} - 3S_n^{i(j+1)k} + 3S_n^{ijk} - S_n^{i(j-1)k}) \\
& - |v_{y_n}^{ijk}|(S_n^{i(j+1)k} - 3S_n^{ijk} + 3S_n^{i(j-1)k} - S_n^{i(j-2)k})\}
\end{aligned} \tag{12}
$$

At the boundary of j, the first order upwind difference scheme is applied as follows:

$$
\begin{aligned}
\frac{\partial(v_{y_n}S)}{\partial y} = & \frac{1}{2\partial y}\{(S_n^{i(j+1)k} + S_n^{ijk})v_{y_n}^{i(j+1)k} - (S_n^{ijk} + S_n^{i(j-1)k})v_{y_n}^{ijk}\} \\
& - \frac{\beta}{2\delta y}\{(S_n^{i(j+1)k} + S_n^{ijk})|v_{y_n}^{i(j+1)k}| - (S_n^{ijk} + S_n^{i(j-1)k})|v_{y_n}^{ijk}|\}
\end{aligned} \tag{13}
$$

where β is a weight constant; $\beta = 1.0$ is adopted in this study. The QUICK scheme is also applied to the third term on the left-hand-side of Eq. (9) and the first order upwind difference is used at the boundary of k. The central difference scheme is applied to the diffraction term of Eq. (9). Consequently, the finite difference version of Eq. (9) finally becomes:

$$
\begin{aligned}
& A_1S_n^{ijk} + A_2S_n^{i(j-2)k} + A_3S_n^{i(j-1)k} + A_4S_n^{i(j+1)k} + A_5S_n^{i(j+2)k} \\
& + A_6S_n^{ij(k-2)} + A_7S_n^{ij(k-1)} + A_8S_n^{ij(k+1)} + A_9S_n^{ij(k+2)} \\
& = -BS_n^{(i-1)jk} \quad (i = 1,\ldots,I;\ j = 1,\ldots,J;\ k = 1,\ldots,K;\ n = 1,\ldots,N)
\end{aligned} \tag{14}
$$

where I and J are the total grid numbers, and K and N are the total numbers of angular and frequency components, respectively. The coefficients in Eq. (14), A_1–A_9 and B, are described in Appendix A.

Since $S_n^{(i-1)jk}$ on the right-hand-side of Eq. (14) are known values, S_n^{ijk} are obtained by solving algebraic equations. In the computer program, boundary conditions such as an open sea boundary, a dissipative beach boundary and a reflecting wall boundary are taken into account as follows.

3.1. Open sea boundary

The spectral density in the cell just outside the calculation area is set to be equal to the value in the cell at the edge of the calculation area:

$$S(x, y + \Delta y, f, \theta) = S(x, y, f, \theta) \tag{15}$$

3.2. Dissipative beach boundary

The spectral density in the cell just outside the computation area is set to be zero:

$$S(x, y + \Delta y, f, \theta) = 0 \tag{16}$$

3.3. Reflecting wall boundary

Fig. 2(a) shows the boundary conditions at a wall for reflection in the y-direction. At a cell immediately adjacent to the sea area, the spectral density is set as

$$S(x, y + \Delta y, f, -\theta + 2\alpha) = K_{ry}^2 S(x, y, f, \theta) \tag{17}$$

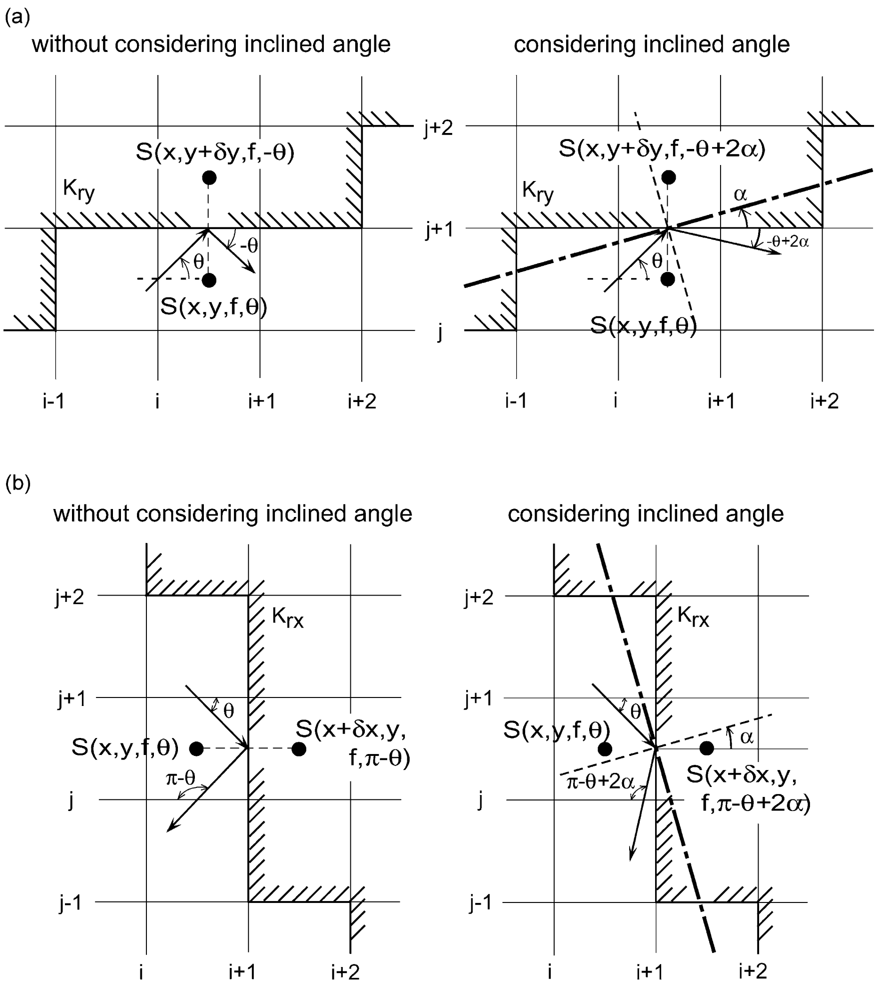

Fig. 2. Reflecting boundaries: (a) reflection in y-direction and (b) reflection in x-direction.

where K_{ry} is the reflection coefficient and α is the angle of the structure (or beach) from the x-axis. For reflection in the x-direction, the source of the reflected spectral density is given as

$$S(x+\Delta x, y, f, \pi-\theta+2\alpha) = K_{rx}^2 S(x, y, f, \theta) \tag{18}$$

where K_{rx} is the reflection coefficient and α is the angle of the normal line to the structure from the x-axis, as shown in Fig. 2(b). It is very important to include the angle of inclination when calculating reflected waves from structures in back-marching calculations. Fig. 3 shows an example calculation for reflected waves from breakwaters; Fig. 3(a) shows the arrangement in which the water depth is constant at 10 m, the incident significant wave height and period are 1.0 m and 10 s, the directional spreading parameter $S_{\max}=25$, the predominant wave direction is 10° off the x-direction, and the reflection coefficient of the breakwaters is set to be 0.9. Fig. 3(b) shows the calculated result for the reflected significant wave height when the orientations of the two breakwaters are not

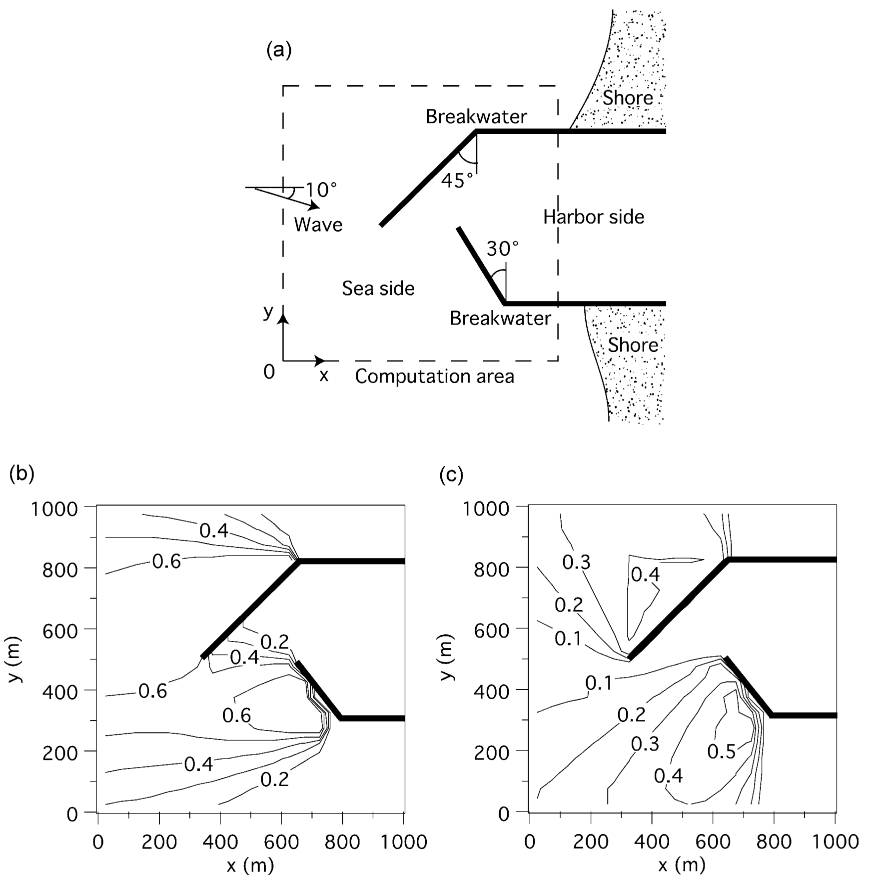

Fig. 3. Calculated results for reflected significant wave heights: (a) calculation arrangement; (b) calculated result without considering orientation of breakwaters; and (c) calculated result considering orientation of breakwaters.

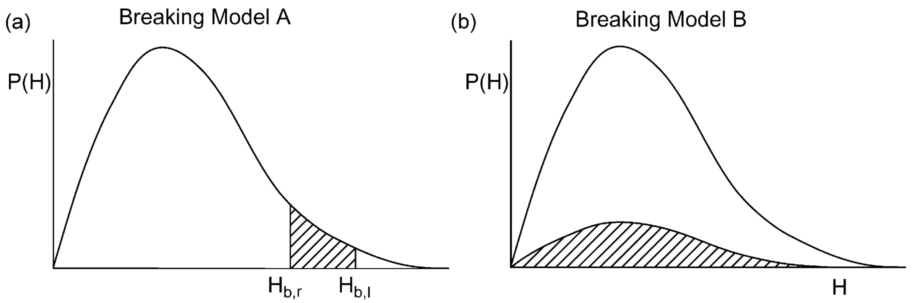

Fig. 4. Energy dissipation model: (a) Takayama et al.'s model (1991) and (b) Thornton and Guza's model (1983).

included in the reflection condition, and Fig. 3(c) gives the result taking the orientations into account. It can be seen that Fig. 3(b) provides more realistic waves than Fig. 3(c).

The energy dissipation coefficient, ε_b, is derived from two different models: Breaking Model A uses Goda's breaking criterion (Takayama et al., 1991); Breaking Model B employs Thornton and Guza's model (1983). Fig. 4 shows schematic explanations of the two breaking models. In both models, the Rayleigh distribution is assumed for the wave height distribution. Breaking Model A uses the breaker height, estimated by Goda's formula, at the right and left hand sides (that is, landward and seaward sides) of a cell, $H_{b,r}$ and $H_{b,l}$. The expected energy dissipation rate can be obtained from the shaded area, sandwiched by $H_{b,r}$ and $H_{b,l}$. In Breaking Model B, the distribution of breaking and broken wave heights is assumed to be proportional to the Rayleigh distribution, as shown by the shaded area in Fig. 4(b). Thornton and Guza (1983) derived the expected energy dissipation rate from the shaded distribution together with the bore dissipation model. The explicit forms of ε_b derived from the two models are given by Takayama et al. (1991) and Thornton and Guza (1983), respectively.

The significant wave height, H_s, the significant wave period, T_s, and the mean wave direction are calculated as follows from the calculated S_n^{ijk}:

$$H_s = 4.0\sqrt{m_0} \tag{19}$$

$$T_s = T_0\sqrt{m_0/m_2}/\bar{T}_0 \tag{20}$$

$$\bar{\theta} = \sum_{n=1}^{N}\sum_{k=1}^{K}\theta_k S_n^{ijk}/m_0 \tag{21}$$

$$m_p = \sum_{n=1}^{N}\sum_{k=1}^{K} f_n^p S_n^{ijk} \tag{22}$$

where T_0 and $\bar{T}_0$ are the incident significant period and mean period, respectively.

Hereafter, the wave model based on the energy balance equation with a diffraction term discretized by the QUICK scheme is designated as the ExEBED model. The wave model described by Mase (2001) using the first order upwind difference scheme is referred to as the EBED model. Finally, the wave models without diffraction, described by Eq. (1), using the first order upwind difference scheme and the QUICK method are called the EBE and ExEBE, respectively.

4. Wave transformation through a gap between breakwaters

4.1. Monochromatic waves

Fig. 5 shows the wave height distributions behind a gap between breakwaters calculated by the ExEBED and EBED models. The water depth is 12 m, the incident wave height is 1 m, the wave period is 10 s, and the incident wave angles, θ, are 30 and 45°. The gap between the breakwaters, B, is divided into 15 cells. The coefficient, κ, in the diffraction term of Eq. (9) is set to be zero in order to investigate the effects of numerical diffusion. The figure shows the wave height distributions at cross sections $x/B=0$ (just behind the breakwaters), 0.2, 0.4 and 0.6. The solid and dotted lines denote the results from the ExEBED and EBED wave models, respectively.

The wave height distribution should remain rectangular as waves propagate through the gap if there is no numerical diffusion. Note, however, that numerical diffusion produces some smoothing. Nevertheless, the ExEBED model shows less smoothing as a result of

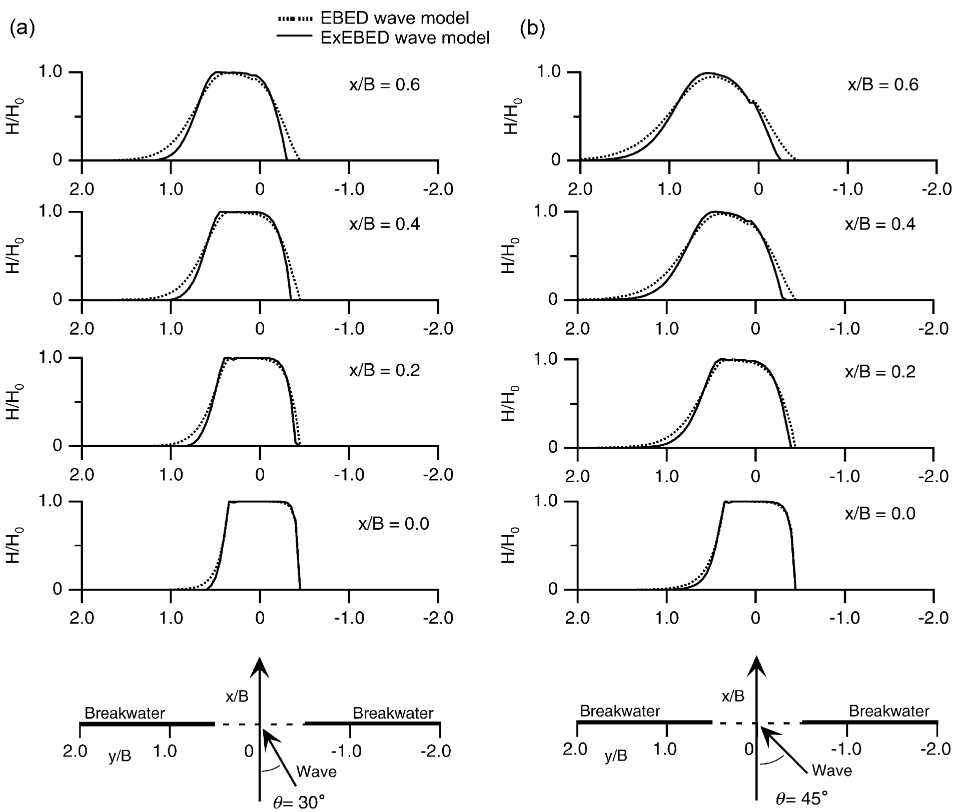

Fig. 5. Heights of monochromatic waves behind a gap in a breakwater: (a) incident angle $\theta=30°$ and (b) incident angle $\theta=45°$.

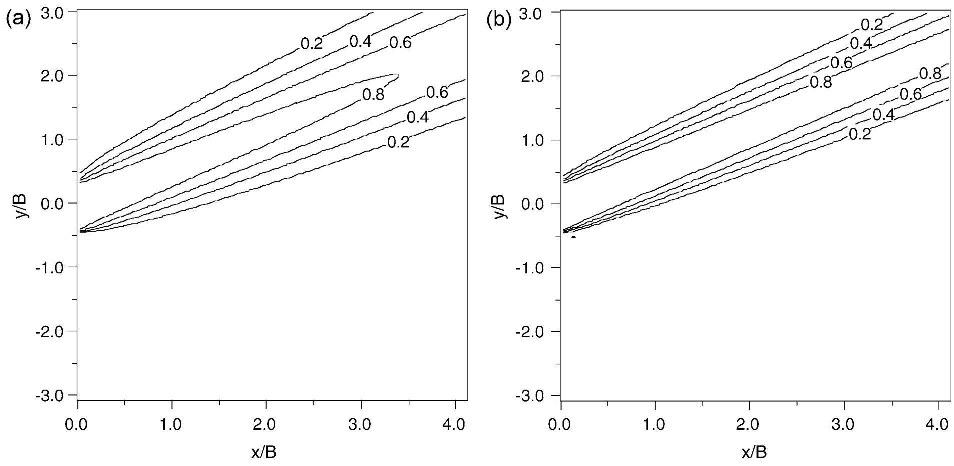

Fig. 6. Contours of wave heights behind a gap in a breakwater: (a) EBED wave model and (b) ExEBED wave model.

numerical diffusion than the EBED wave model, though the difference appears small. As the incident wave angle increases, so also does the degree of numerical diffusion.

Fig. 6 shows the contours of wave height for an incident wave angle of $\theta = 30°$. As expected, the contours spread gradually with increase in propagation distance. However, the spread of the contours is narrower for the ExEBED model than for the EBED wave model.

4.2. Multidirectional random waves

When the gap between breakwaters is wide and the incident random waves have a broad angular spread, the EBE model agrees well with the Sommerfeld solutions (Takayama et al., 1991). However, for a narrow gap and waves with a limited angular spread, there is poor agreement between this model and the Sommerfeld results.

Here, the ExEBED model is compared with the results of the Sommerfeld theory for different values of the coefficient κ in the diffraction term. The water depth is 12 m, the incident significant wave height and period are 1 m and 10 s, respectively, the energy spectrum is of JONSWAP form with a peak enhancement factor of $\gamma = 3.3$ and the wave directional spreading function is of the Mitsuyasu type with peak values of $S_{\max} = 10$, 25 and 75. The gap width B varies from $B/L = 2$ to $B/L = 8$, where L ($= 100$ m) is the wavelength. The grid sizes δx and δy are $B/20$, the number of component waves (of equal energy with different frequency bands) is 10 and the number of component angles is 36. The error, Err, in the model predictions is defined as follows:

$$\mathrm{Err} = \frac{\sum_i \sum_j (H_{\mathrm{t}\,ij} - H_{\mathrm{c}\,ij})^2}{\sqrt{\sum_i \sum_j H_{\mathrm{t}\,ij}^2}\sqrt{\sum_i \sum_j H_{\mathrm{c}\,ij}^2}} \tag{23}$$

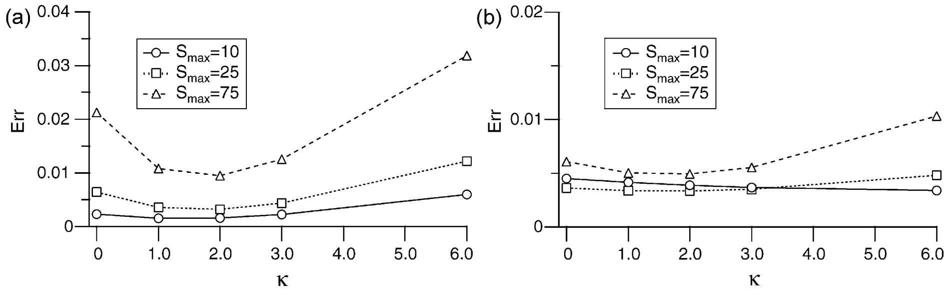

Fig. 7. Error as a function of κ: (a) $B/L=2$ and (b) $B/L=8$.

in which H_t and H_c represent Sommerfeld's theoretical results and the calculated values of significant wave height, respectively, and (i,j) are the grid numbers.

Fig. 7 shows the errors as a function of the coefficient κ in the diffraction term. The influence of angular spreading is shown by changing the spreading parameter S_{max}. In Fig. 7(a), for $B/L=2$, the errors are minimized when $\kappa=2.0$, irrespective of the value of S_{max}. In Fig. 7(b), for the case of $B/L=8$, the error is also minimized for $S_{max}=75$ when $\kappa=2.0$. For the other two spreading parameters, the errors remain small regardless of κ. For these reasons, $\kappa=2.0$ is adopted hereafter. Note that this value is a little smaller than that used in Mase (2001).

Fig. 8 compares the calculated significant wave heights obtained from the EBE model with the results of Sommerfeld's theory for the case of $B/L=2$ for $S_{max}=25$ and 75. The solid lines denote the calculated results and the dotted lines are the Sommerfeld solutions. For this case of a narrow gap, the agreement between the calculated values and Sommerfeld's theory is poor for all values of S_{max}. Predictions from the ExEBED model

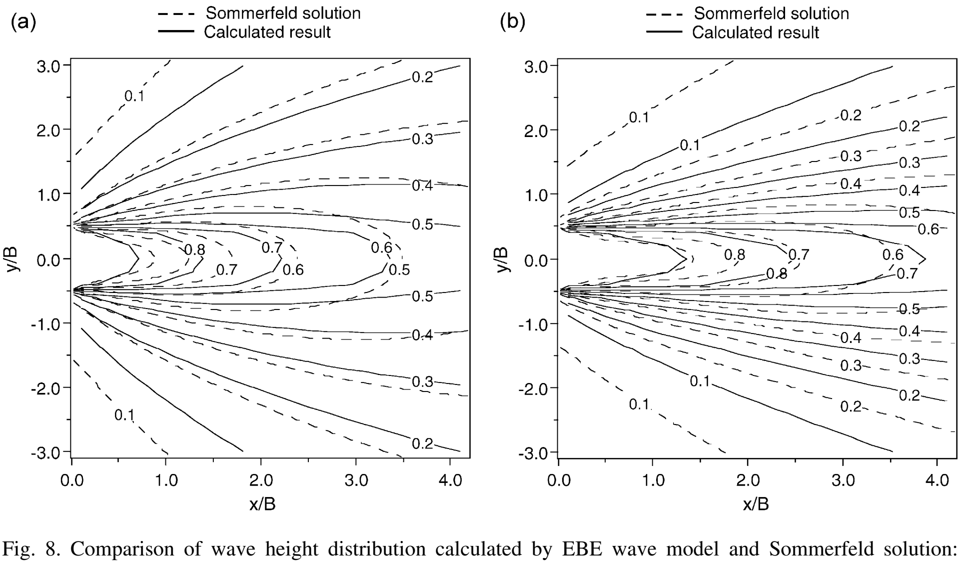

Fig. 8. Comparison of wave height distribution calculated by EBE wave model and Sommerfeld solution: (a) $B/L=2$, $S_{max}=25$ and (b) $B/L=2$, $S_{max}=75$.

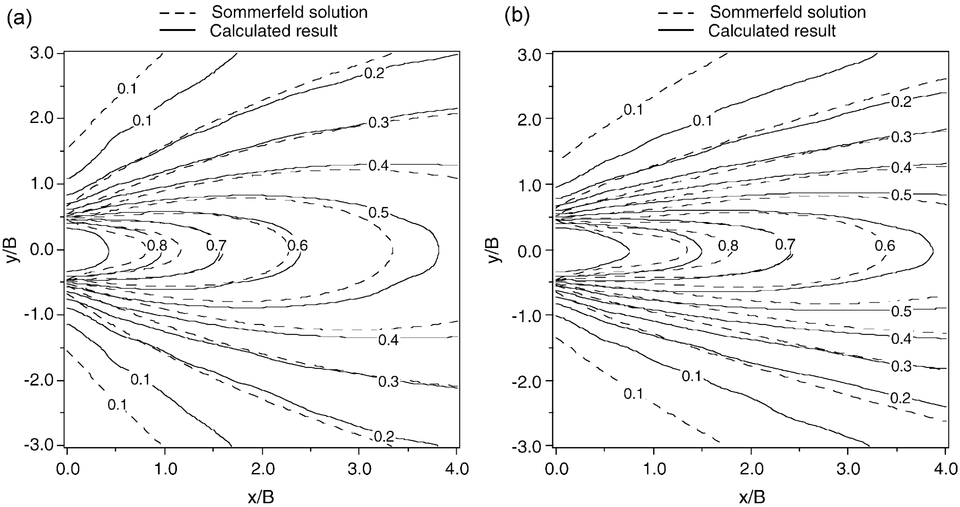

Fig. 9. Comparison of wave height distribution calculated by ExEBED wave model and Sommerfeld solution: (a) $B/L=2$, $S_{max}=25$ and (b) $B/L=2$, $S_{max}=75$.

for the same cases are compared with Sommerfeld's theory in Fig. 9. Here, agreement is much better except near the gap and immediately behind the breakwaters where the wave heights are small. Finally, Fig. 10 shows the diffraction coefficient K_d $(=H_s/(H_s)_0)$ at cross-sections $x/B=1$–3. The broken lines are Sommerfeld's solutions, the dotted lines represent results from the EBE model, and the solid lines are the results from the ExEBED wave model.

From the evidence of Figs. 8–10, the ExEBED appears to be better than the EBE model, whilst predictions from the ExEBED and EBED models are almost the same if suitable values are adopted for coefficient κ in the diffraction term, accounting for the reduction in numerical diffusion provided by the ExEBED.

5. Wave transformation due to a circular shoal

In this section, results from the ExEBED wave model are compared with Chawla et al.'s (1998) experimental data on wave transformation due to a circular shoal. The shoal, with a radius of 2.57 m and a height of 0.37 m, was installed in a constant water depth of 0.4 m. A schematic view of the experimental setup and measurement positions is provided in Fig. 11. Although seven transects were utilized in the experiments, wave height distributions along four transects, denoted by the broken lines are used in this study. The centre of the shoal (x_c, y_c) was at (5.0 m, 8.98 m). The wave-making paddles were along the line $x=0$ m. The random waves used in the experiments had a TMA spectrum and angular spreading was simulated by using a wrapped normal spreading function. There were two incident wave heights and two degrees of angular spreading. In all four cases, the waves broke on top of the shoal.

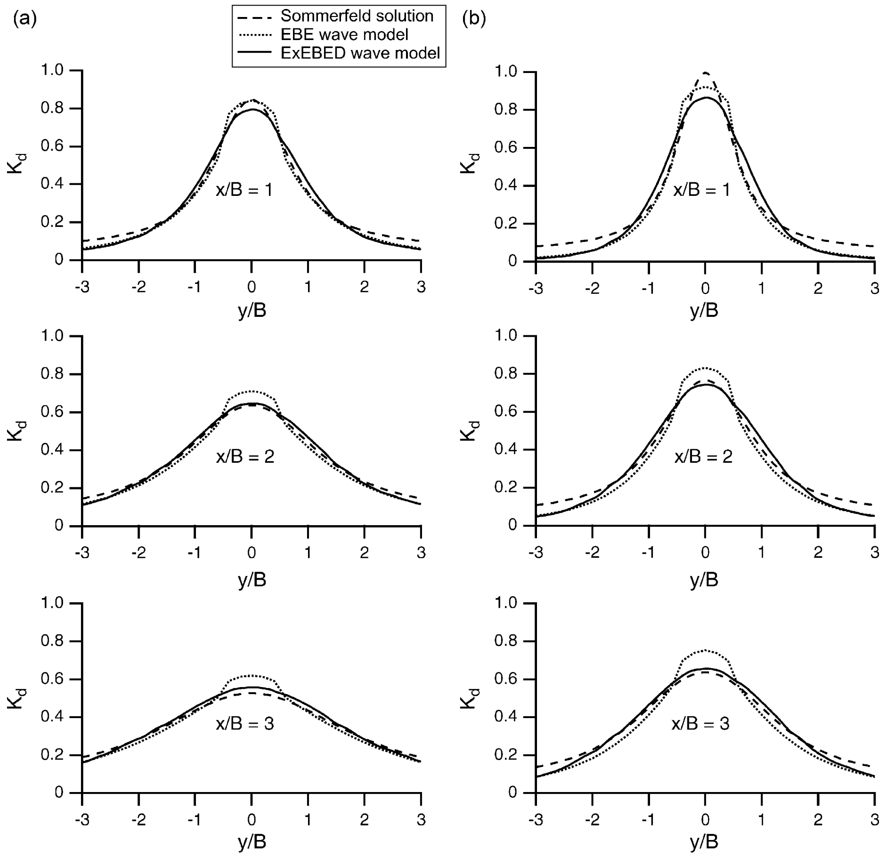

Fig. 10. Wave height distributions at three sections: (a) $B/L=2$, $S_{max}=25$ and (b) $B/L=2$, $S_{max}=75$.

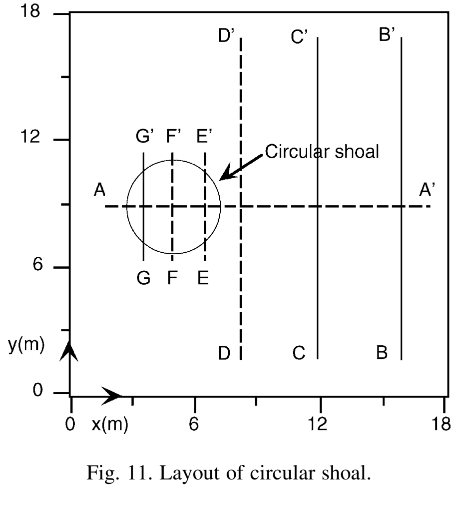

Fig. 11. Layout of circular shoal.

In the present calculations, the grid size was set to be 0.1 m, the number of frequency components was 20, the number of component angles was 36 and the coefficient κ in the diffraction term was taken as 2.0. Fig. 12 shows the normalized significant wave heights along the four measurement lines for Test 3, where the incident waves were small and angular spreading was narrow. The dotted and solid lines represent the calculated wave

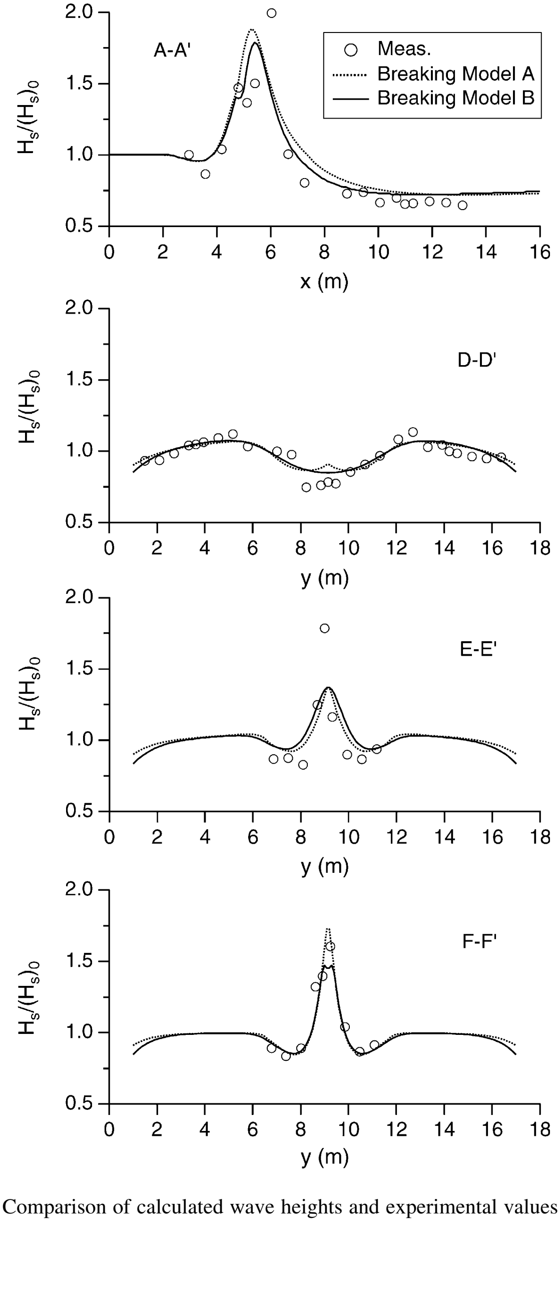

Fig. 12. Comparison of calculated wave heights and experimental values (Test 3).

heights using the energy dissipation of Breaking Models A and B, respectively, and the solid circles are the measurements. Both forms of the ExEBED wave model underestimate the sharp peak in the measured wave heights at cross-section $E–E'$, and there is a difference between the positions of the peaks in wave height at section $A–A'$. Otherwise, calculated results are almost the same except around $y=9$ m at section $E–E'$ and around $x=5$ m at section $A–A'$.

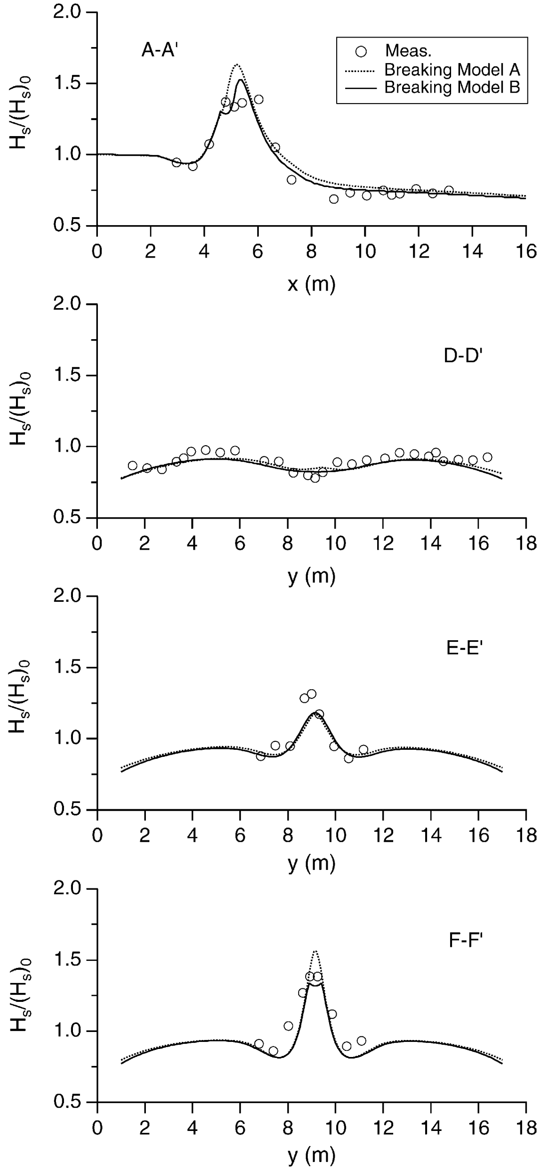

Fig. 13. Comparison of calculated wave heights and experimental values (Test 4).

Fig. 13 shows the normalized significant wave heights for Test 4, where the incident waves were small and the angular spreading was wide. At section E–E', the predictions are somewhat smaller than the measurements at the peak in wave height; except for this point, there is good agreement when using Breaking Model B. On the other hand, the wave model (REF/DIF S) used by Chawla et al. (1998) overpredicted the peak in wave heights at

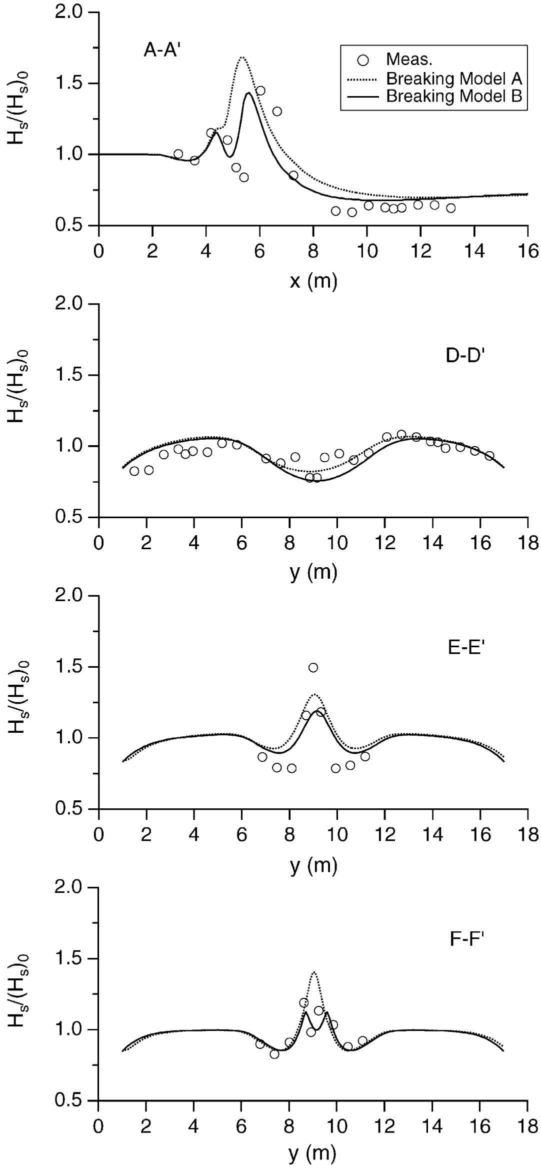

Fig. 14. Comparison of calculated wave heights and experimental values (Test 5).

section E–E'. At section A–A', the ExEBED results using Breaking Model B are better around $x = 5$ m than the results using Breaking Model A.

The case of large incident waves and narrow spreading is shown in Fig. 14. In this case, severe wave breaking occurred. At cross section A–A', there are small measured wave heights around $x = 5.5$ m. The predictions using Breaking Model A do not show this drop

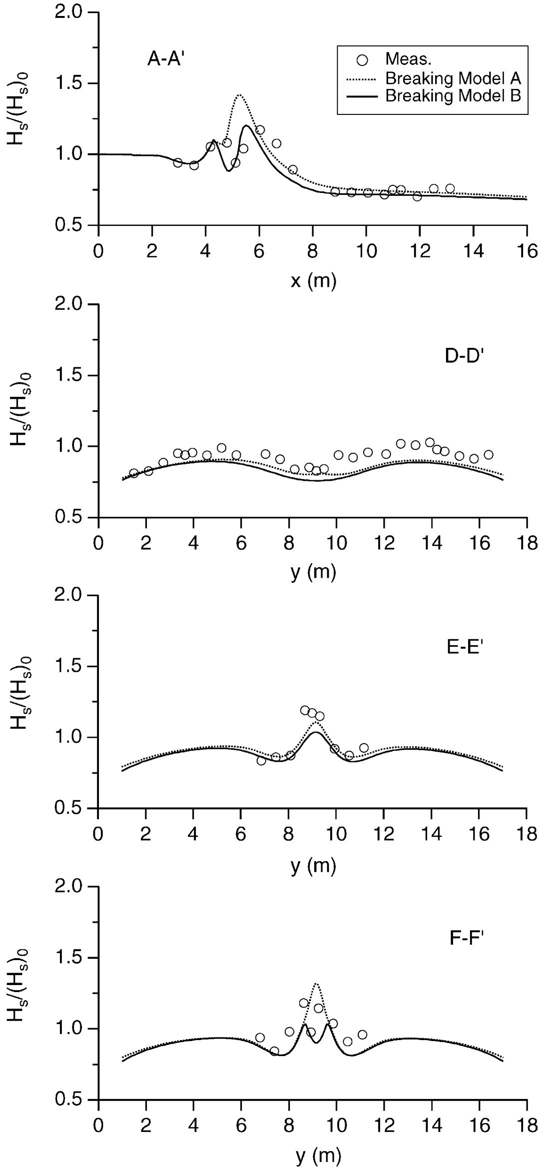

Fig. 15. Comparison of calculated wave heights and experimental values (Test 6).

in wave heights. However, although the predictions using Breaking Model B show the wave height drop, there is a problem in reproducing the large wave height at $y=9$ m at section E–E'.

Finally, Fig. 15 compares the predictions and measurements for Test 6 involving large incident waves and a wide angular spread. Again, the small wave heights around $x=5.0$ m at section A–A' are not reproduced by the ExEBED using Breaking Model A. The experiments show a double peak in the wave height distribution. Nevertheless, although there are some differences between the experimental data and the ExEBED wave model using Breaking Model B, Figs. 12–15 suggest that the ExEBED using this breaking model generally provides good results.

6. Wave transformation at a field site

Fig. 16 shows the bathymetry to which the wave prediction models were applied. In the figure, the symbol ‘O’ denotes the location of the offshore wave measurements and the symbol ‘X’ denotes the wave gauge behind the breakwater. Eleven sets of wave data were

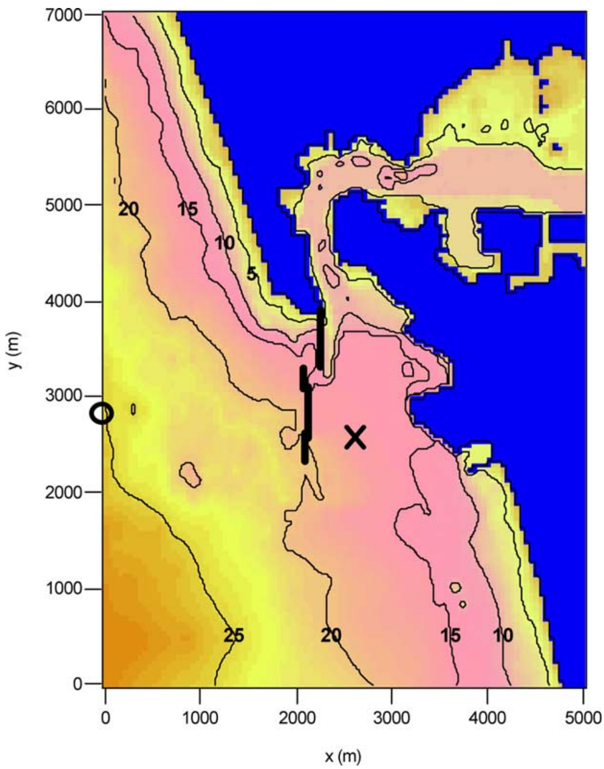

Fig. 16. Field bathymetry.

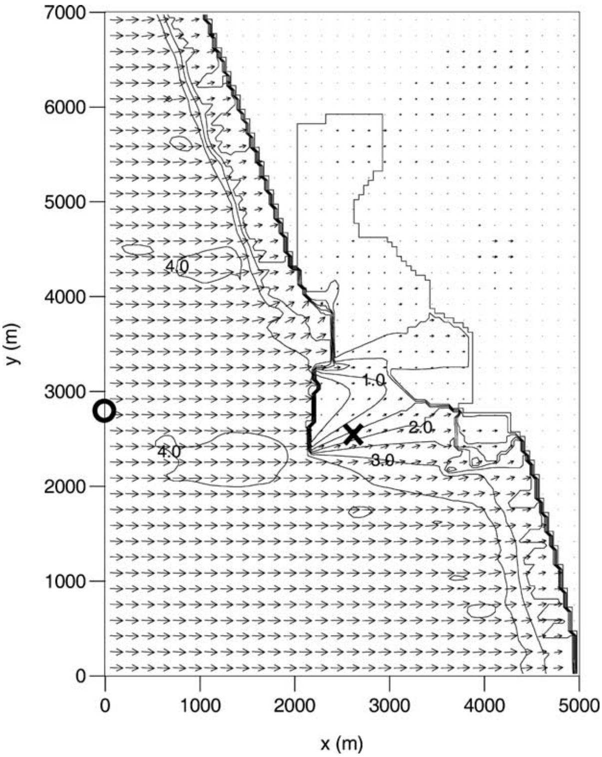

Fig. 17. Calculated result of spatial wave height distribution by the ExEBED.

used: the significant heights at the offshore point ranged from 3.5 to 5.5 m, the significant periods from 11 to 14 s, and the main incident angles from -2 to $-10°$.

A calculated result for the wave height distribution, shown by contour lines and a vector plot, is shown in Fig. 17 where the incident waves have $H_s=4.0$ m, $T_s=11$ s, $\theta=0°$, and $S_{max}=25$. Fig. 18 compares the measured wave heights with the calculated values using the EBE, EBED, ExEBE and ExEBED models. Generally, predicted values lie in the range $\pm 40\%$ of the measured values. However, it is hard to say, from Fig. 18, which wave model is best. The differences between predictions by the four wave models are not large and the agreement between the observations and the predictions provided by all of the models is fairly good. Generally speaking, if diffraction effects are included, the wave heights behind the breakwater are larger, as would be expected.

7. Conclusions

This study extends an energy-balance-equation wave model for multidirectional random wave transformations to account for the effect of wave diffraction and to reduce

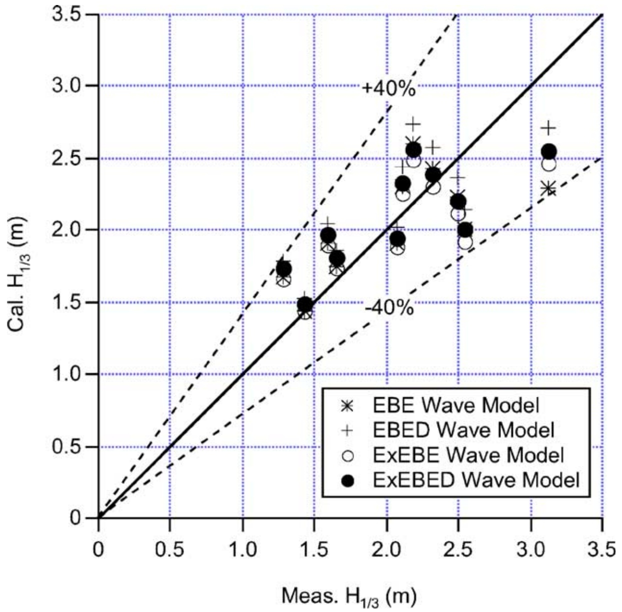

Fig. 18. Comparison of observations and predictions for waves at a field site.

numerical diffusion. The predictions by the wave model based on the energy-balance-equation with diffraction (the ExEBED wave model) were validated against the results of Sommerfeld's theory for wave transformation through a gap between breakwaters. It was also validated against Chawla et al.'s (1998) measurements of wave conditions around a circular shoal and against field observations.

The ExEBED wave model has less numerical diffusion than the EBE wave model using the first order upwind scheme. Comparison of its predictions, using Thornton and Guza's breaking model, with the measurements by Chawla et al. (1998) showed that although there are some differences, particularly where the wave height distribution is sharply peaked due to wave focusing or where it decreases abruptly due to wave breaking, measured and predicted values are in generally satisfactory agreement. Concerning the field results, the agreement between observations and predictions using ExEBED is fairly good. Generally speaking, the predicted wave heights behind the breakwater are larger, if diffraction effects are included.

Acknowledgements

A part of this study was supported by the Joint Research Project under the Japan–China Scientific Cooperation Program (Project Name: Development of a practical system for health monitoring and vibration control of offshore platforms considering marine conditions of storm surge and waves). The first author is grateful to the Ministry of Education, Culture, Sports, Science and Technology, Japan, for its support during his stay

as an Overseas Research Scholar in the Department of Civil Engineering, University of Liverpool, United Kingdom.

Appendix A. Coefficients in Eq. (14)

The coefficients in Eq. (14), A_1–A_9 and B, are as follows:

$$A_1 = v_{x_n}^{(i+1)jk}/\delta x + \varepsilon_{b_n}^{ij} + \frac{\kappa}{2\omega_n \delta y^2}\{(CC_g)^{i(j+1)k} + (CC_g)^{ijk} - (CC_g)^{i(j+1/2)k}\}\cos^2\theta_k + \frac{1}{16\delta y}\{9v_{y_n}^{i(j+1)k} - 9v_{y_n}^{ijk} + 3\eta|v_{y_n}^{i(j+1)k}| + 3\eta|v_{y_n}^{ijk}|\} + \frac{1}{16\delta\theta}\{9v_{\theta_n}^{ij(k+1)} - 9v_{\theta_n}^{ijk} + 3\eta|v_{\theta_n}^{ij(k+1)}| + 3\eta|v_{\theta_n}^{ijk}|\} \quad \text{(A1)}$$

$$A_2 = \frac{1}{16\delta y}\{v_{y_k}^{ijk} + \eta|v_{y_n}^{ijk}|\} \quad \text{(A2)}$$

$$A_3 = -\frac{1}{16\delta y}\{v_{y_n}^{i(j+1)k} + 9v_{y_n}^{ijk} + \eta|v_{y_n}^{i(j+1)k}| + 3\eta|v_{y_n}^{ijk}|\} + \frac{\kappa}{2\omega_n \delta y^2}\left\{-(CCg)^{ijk} + \frac{1}{2}(CCg)^{i\left(j+\frac{1}{2}\right)k}\right\}\cos^2\theta_k \quad \text{(A3)}$$

$$A_4 = \frac{1}{16\delta y}\{9v_{y_n}^{i(j+1)k} + v_{y_n}^{ijk} - 3\eta|v_{y_n}^{i(j+1)k}| - \eta|v_{y_n}^{ijk}|\} + \frac{\kappa}{2\omega_n \delta y^2}\left\{-(CCg)^{i(j+1)k} + \frac{1}{2}(CCg)^{i\left(j+\frac{1}{2}\right)k}\right\}\cos^2\theta_k \quad \text{(A4)}$$

$$A_5 = \frac{1}{16\delta y}\{-v_{y_n}^{i(j+1)k} + \eta|v_{y_n}^{i(j+1)k}|\} \quad \text{(A5)}$$

$$A_6 = \frac{1}{16\delta\theta}\{v_{\theta_n}^{ijk} + \eta|v_{\theta_n}^{ijk}|\} \quad \text{(A6)}$$

$$A_7 = -\frac{1}{16\delta\theta}\{v_{\theta_n}^{ij(k+1)} + 9v_{\theta_n}^{ijk} + \eta|v_{\theta_n}^{ij(k+1)}| + 3\eta|v_{\theta_n}^{ijk}|\} \quad \text{(A7)}$$

$$A_8 = \frac{1}{16\delta\theta}\{9v_{\theta_n}^{ij(k+1)} + v_{\theta_n}^{ijk} - 3\eta|v_{\theta_n}^{ij(k+1)}| - \eta|v_{\theta_n}^{ijk}|\} \quad \text{(A8)}$$

$$A_9 = \frac{1}{16\delta\theta}\{-v_{\theta_n}^{ij(k+1)} + \eta|v_{\theta_n}^{ij(k+1)}|\} \quad \text{(A9)}$$

$$B = v_{x_n}^{ijk}/\delta x \tag{A10}$$

At the boundaries of j or k, the following coefficients are used.

(1) Both j and k are on the boundary:

$$A_1 = v_{x_n}^{(i+1)jk}/\delta x + \varepsilon_{b_n}^{ij} + \frac{\kappa}{2\omega_n \delta y^2}\{(CC_g)^{i(j+1)k} + (CC_g)^{ijk} - (CC_g)^{i(j+1/2)k}\}\cos^2\theta_k + \frac{1}{2\delta y}\{v_{y_n}^{i(j+1)k} - v_{y_n}^{ijk} + \eta|v_{y_n}^{i(j+1)k}| + \eta|v_{y_n}^{ijk}|\} + \frac{1}{2\delta\theta}\{v_{\theta_n}^{ij(k+1)} - v_{\theta_n}^{ijk} + \eta|v_{\theta_n}^{ij(k+1)}| + \eta|v_{\theta_n}^{ijk}|\} \tag{A11}$$

$$A_3 = -\frac{1}{2\delta y}\{v_{y_n}^{ijk} + \eta|v_{y_n}^{ijk}|\} + \frac{\kappa}{2\omega_n\delta y^2}\left\{-(CCg)^{ijk} + \frac{1}{2}(CCg)^{i(j+\frac{1}{2})k}\right\}\cos^2\theta_k \tag{A12}$$

$$A_4 = \frac{1}{2\delta y}\{v_{y_n}^{i(j+1)k} - \eta|v_{y_n}^{i(j+1)k}|\} + \frac{\kappa}{2\omega_n\delta y^2}\left\{-(CCg)^{i(j+1)k} + \frac{1}{2}(CCg)^{i(j+\frac{1}{2})k}\right\}\cos^2\theta_k \tag{A13}$$

$$A_7 = -\frac{1}{2\delta\theta}\{v_{\theta_n}^{ijk} + \eta|v_{\theta_n}^{ijk}|\} \tag{A14}$$

$$A_8 = \frac{1}{2\delta\theta}\{v_{\theta_n}^{ij(k+1)} - \eta|v_{\theta_n}^{ij(k+1)}|\} \tag{A15}$$

$$A_2 = A_5 = A_6 = A_9 = 0 \tag{A16}$$

$$B = v_{x_n}^{ijk}/\delta x \tag{A17}$$

(2) Only j is on the boundary:

$$A_1 = v_{x_n}^{(i+1)jk}/\delta x + \varepsilon_{b_n}^{ij} + \frac{\kappa}{2\omega_n \delta y^2}\{(CC_g)^{i(j+1)k} + (CC_g)^{ijk} - (CC_g)^{i(j+1/2)k}\}\cos^2\theta_k + \frac{1}{2\delta y}\{v_{y_n}^{i(j+1)k} - v_{y_n}^{ijk} + \eta|v_{y_n}^{i(j+1)k}| + \eta|v_{y_n}^{ijk}|\} + \frac{1}{16\delta\theta}\{9v_{\theta_n}^{ij(k+1)} - 9v_{\theta_n}^{ijk} + 3\eta|v_{\theta_n}^{ij(k+1)}| + 3\eta|v_{\theta_n}^{ijk}|\} \tag{A18}$$

$$A_3 = -\frac{1}{2\delta y}\{v_{y_n}^{ijk} + \eta|v_{y_n}^{ijk}|\} + \frac{\kappa}{2\omega_n\delta y^2}\left\{-(CCg)^{ijk} + \frac{1}{2}(CCg)^{i\left(j+\frac{1}{2}\right)k}\right\}\cos^2\theta_k \tag{A19}$$

$$A_4 = \frac{1}{2\delta y}\{v_{y_n}^{i(j+1)k} - \eta|v_{y_n}^{i(j+1)k}|\} + \frac{\kappa}{2\omega_n\delta y^2}\left\{-(CCg)^{i(j+1)k} + \frac{1}{2}(CCg)^{i\left(j+\frac{1}{2}\right)k}\right\}\cos^2\theta_k \tag{A20}$$

$$A_6 = \frac{1}{16\delta\theta}\{v_{\theta_n}^{ijk} + \eta|v_{\theta_n}^{ijk}|\} \tag{A21}$$

$$A_7 = -\frac{1}{16\delta\theta}\{v_{\theta_n}^{ij(k+1)} + 9v_{\theta_n}^{ijk} + \eta|v_{\theta_n}^{ij(k+1)}| + 3\eta|v_{\theta_n}^{ijk}|\} \tag{A22}$$

$$A_8 = \frac{1}{16\delta\theta}\{9v_{\theta_n}^{ij(k+1)} + v_{\theta_n}^{ijk} - 3\eta|v_{\theta_n}^{ij(k+1)}| - \eta|v_{\theta_n}^{ijk}|\} \tag{A23}$$

$$A_9 = \frac{1}{16\delta\theta}\{-v_{\theta_n}^{ij(k+1)} + \eta|v_{\theta_n}^{ij(k+1)}|\} \tag{A24}$$

$$A_2 = A_5 = 0 \tag{A25}$$

$$B = v_{x_n}^{ijk}/\delta x \tag{A26}$$

(3) Only k is on the boundary:

$$A_1 = v_{x_n}^{(i+1)jk}/\delta x + \varepsilon_{b_n}^{ij} + \frac{\kappa}{2\omega_n\delta y^2}\{(CC_g)^{i(j+1)k} + (CC_g)^{ijk} - (CC_g)^{i(j+1/2)k}\}\cos^2\theta_k + \frac{1}{2\delta y}\{v_{y_n}^{i(j+1)k} - v_{y_n}^{ijk} + \eta|v_{y_n}^{i(j+1)k}| + \eta|v_{y_n}^{ijk}|\} + \frac{1}{16\delta\theta}\{9v_{\theta_n}^{ij(k+1)} - 9v_{\theta_n}^{ijk} + 3\eta|v_{\theta_n}^{ij(k+1)}| + 3\eta|v_{\theta_n}^{ijk}|\} \tag{A27}$$

$$A_2 = \frac{1}{16\delta y}\{v_{y_n}^{ijk} + \eta|v_{y_n}^{ijk}|\} \tag{A28}$$

$$A_3 = \frac{1}{16\delta y}\{v_{y_n}^{i(j+1)k} + 9v_{y_n}^{ijk} + \eta|v_{y_n}^{i(j+1)k}| + 3\eta|v_{y_n}^{ijk}|\} + \frac{\kappa}{2\omega_n\delta y^2}\left\{-(CCg)^{ijk} + \frac{1}{2}(CCg)^{i\left(j+\frac{1}{2}\right)k}\right\}\cos^2\theta_k \tag{A29}$$

$$A_4 = \frac{1}{16\delta y}\{9v_{y_n}^{i(j+1)k} + v_{y_n}^{ijk} - 3\eta|v_{y_n}^{i(j+1)k}| - \eta|v_{y_n}^{ijk}|\}$$

$$+ \frac{\kappa}{2\omega_n\delta y^2}\left\{-(CCg)^{i(j+1)k} + \frac{1}{2}(CCg)^{i(j+\frac{1}{2})k}\right\}\cos^2\theta_k \tag{A30}$$

$$A_5 = \frac{1}{16\delta y}\{-v_{y_n}^{i(j+1)k} + \eta|v_{y_n}^{i(j+1)k}|\} \tag{A31}$$

$$A_7 = -\frac{1}{2\delta\theta}\{v_{\theta_n}^{ijk} + \eta|v_{\theta_n}^{ijk}|\} \tag{A32}$$

$$A_8 = \frac{1}{2\delta\theta}\{v_{\theta_n}^{ij(k+1)} - \eta|v_{\theta_n}^{ij(k+1)}|\} \tag{A33}$$

$$A_6 = A_9 = 0 \tag{A34}$$

$$B = v_{x_n}^{ijk}/\delta x \tag{A35}$$

References

Booij, N., Holthuijsen, L.H., Ris, R.C., 1996. The 'SWAN' wave model for shallow water. Proceedings of the 25th International Conference on Coastal Engineering, ASCE, New York, pp 668–676.

Booij, N., Holthuijsen, L.H., Doorn, N., Kieftenburg, A.T.M.M., 1997. Diffraction in a spectral wave model. Proceedings of the Third International Symposium Waves'97, ASCE, New York, pp 243–255.

Chawla, A., Özkan, H.T., Kirby, J.T., 1998. Spectral model for wave transformation and breaking over irregular bathymetry. J. Waterways, Port, Coast., Ocean Eng., ASCE 124 (4), 189–198.

Gobbi, M.F., Kirby, J.T., 1999. Wave evolution over submerged sills: tests of a high-order Boussinesq model. Coast. Eng. 37, 57–96.

Holthuijsen, L.H., Herman, A., Booij, N., 2003. Phase-decoupled refraction–diffraction for spectral wave model. Coast. Eng. 49, 291–305.

Kaihatu, J.M., Kirby, J.T., 1998. Two-dimensional parabolic modeling of extended Boussinesq equations. J. Waterway, Port, Coast. Ocean Eng., ASCE 124 (2), 57–67.

Kirby, J.T., Dalrymple, R.A., 1986. Modeling waves in surfzones and around islands. J. Waterway, Port, Coast., Ocean Eng. 112 (1), 78–93.

Leonard, B.P., 1979. A stable and accurate convective modelling procedure based on quadratic upstream interpolation. Comput. Meth. Appl. Mech. Eng. 19, 59–98.

Madsen, P.A., Murray, R., Sorensen, O.R., 1991. A new form of the Boussinesq equations with improved linear dispersion characteristics. Coast. Eng. 15 (4), 371–388.

Madsen, P.A., Sorensen, O.R., Schaffer, H.A., 1997a. Surf zone dynamics simulated by a Boussinesq type model. Part I: Model description and cross-shore motion of regular waves. Coast. Eng. 32, 255–287.

Madsen, P.A., Sorensen, O.R., Schaffer, H.A., 1997b. Surf zone dynamics simulated by a Boussinesq type model. Part II: surf beat and swash oscillations for wave groups and irregular waves. Coast. Eng. 32, 289–319.

Mase, H., 2001. Multidirectional random wave transformation model based on energy balance equation. Coast. Eng. J. 43 (4), 317–337.

Mase, H., Kitano, T., 2000. Spectrum-based prediction model for random wave transformation over arbitrary bottom topography. Coast. Eng. J. 42 (1), 111–151.

Nwogu, O., 1993. A alternative form of the Boussinesq equations for nearshore wave propagation. J. Waterway, Port, Coast., Ocean Eng., ASCE 119 (6), 618–638.

Peregrine, D.H., 1967. Long waves on a beach. J. Fluid Mech. 27 (4), 815–827.

Radder, A.C., 1979. On the parabolic equation method for water wave propagation. J. Fluid Mech. 95 (1), 159–176.

Resio, D.T., 1988. A steady-state wave model for coastal applications. Proceedings of the 21st International Conference on Coastal Engineering, ASCE, New York, pp. 929–940.

Rivero, F.J., Arcilla, A.S., Carci, E., 1997. An analysis of diffraction in spectral wave models. Proceedings of the Third International Symposium on Waves'97, ASCE, New York, pp. 431–435.

Takayama, T., Ikeda, N., Hiraishi, T., 1991. Wave transformation calculation considering wave breaking and reflection. Rept. Port Harbor Res. Inst. 30 (1), 21–67.

Thornton, E.B., Guza, R.T., 1983. Transformation of wave height distribution. J. Geophys. Res. 88 (C10), 5925–5938.

WAMDI group, 1988. The WAM model—a third generation ocean wave prediction model. J. Phys. Oceanogr. 18, 1775–1810.

Wei, G., Kirby, J.T., Grilli, S.T., Subramanya, R., 1995. A fully nonlinear Boussinesq model for surface waves. Part 1: Highly nonlinear unsteady waves. J. Fluid Mech. 29, 471–492.